Available online at www.sciencedirect.com
SCIENCE DIRECT®
Acta Materialia 53 (2005) 87–96
Acta MATERIALIA
www.actamat-journals.com

Computational study of carbon segregation and diffusion within a nickel grain boundary

Donald J. Siegel *, J.C. Hamilton

Department of Materials Physics, Sandia National Laboratories, Mail Stop 9161, Livermore, CA 94551, USA

Received 24 May 2004; received in revised form 25 August 2004; accepted 12 September 2004
Available online 26 October 2004

Abstract

Using density functional theory, we study the segregation and diffusion of carbon interstitials at a nickel $\Sigma 3$ $(1\,1\,\bar{2})$ tilt grain boundary (GB) as a function of C coverage and Ni magnetic state. We find that segregation is most favorable for a "checkerboard" configuration at a coverage of $\frac{1}{2}$ monolayer in both non-magnetic (NM) and ferromagnetic (FM) states, with FM (NM) heats of segregation approaching -0.5 (-0.3) eV per C atom. Segregation is 0.1–0.2 eV stronger in the FM state, because C interstitials suppress Ni magnetism, and this suppression is minimized when C resides at the boundary. Carbon GB diffusion is predicted to be highly anisotropic: calculated energy barriers (E_a) for migration parallel to the $[1\,\bar{1}\,0]$ tilt axis are significantly smaller (E_a = 0.44–0.77 eV) than for lattice diffusion (E_a = 1.62 eV), while barriers perpendicular to $[1\,\bar{1}\,0]$ are comparable to those of lattice diffusion. Changes in barrier height due to Ni magnetism are (with one exception) relatively small, and are evident only when the diffusion pathway bisects highly compressed GB sites.

Keywords: Grain boundary segregation; Grain boundary diffusion; Magnetic properties; Nickel alloys; First-principles electron theory

1. Introduction

The properties of crystalline materials, while dependent upon their overall composition, are determined in large part by their microstructure. Grain boundaries (GB), in particular, are known to have a significant impact upon the macroscopic properties of polycrystalline solids [1], as they can support higher concentrations of point defects, and can exhibit lower activation energies for diffusion [2] in comparison to the bulk lattice. The favorable mechanical properties of nanocrystalline materials, which are characterized by a high volume density of GBs, further highlights the need to understand and control the fundamental properties of these internal interfaces.

Pioneering experimental work by Hoffman [3], along with later studies by Sommer and co-workers [4], have demonstrated some of the unusual properties of GBs in metals. In particular, they have shown that GB self-diffusion in oriented silver bicrystals is generally anisotropic – both for low- and high-angle boundaries – with diffusion occurring most rapidly along the [0 0 1] tilt axis. Experiments performed by Parthasarathy and Shewmon [5] on the diffusion of C interstitials along Ni GBs revealed that boundary diffusion was four orders of magnitude faster than lattice diffusion. In addition, atom probe field-ion microscopy experiments performed by von Alvensleben [6] on Ni–1 at.% C alloys found high concentrations of segregated C (25–35 at.%) at two grain boundaries.

While experimental techniques can readily measure the impact of GBs on materials properties, they are less

* Corresponding author. Center for Computational Materials Science, Naval Research Laboratory, Code 6390, 4555 Overlook Ave SW, Washington, DC 20375, USA. Tel.: +1 202 404 4404; fax: +1 202 404 7546.
E-mail address: dsiegel@dave.nrl.navy.mil (D.J. Siegel).

1359-6454/$30.00
doi:10.1016/j.actamat.2004.09.006

well suited to probe the atomic-scale mechanisms and structures which underly these effects. In this regard, atomistic computer simulations based mostly upon (semi-)empirical potentials have proven invaluable, and have rapidly grown in complexity [7–10]. The primary advantage of these methods is their low computational cost, which is beneficial for modeling complex processes such as diffusion.

One of the first atomistic studies of GB segregation was performed by Foiles [11], in which embedded-atom method (EAM) potentials were used in conjunction with Monte-Carlo simulations to model segregation to symmetric twist boundaries in Ni–Cu alloys. Rittner and Seidman [12] later investigated the segregation of Pd to 21 symmetric ⟨1 1 0⟩ tilt boundaries in Ni. Regarding GB diffusion, Sörensen and co-workers [13] recently performed a detailed EAM study of self-diffusion mechanisms within two symmetric tilt (Σ5) boundaries in Cu by combining a variety of techniques. This, and related work by Suzuki and Mishin [14], have identified new diffusion mechanisms involving the concerted motion of multiple atoms.

However, one of the drawbacks regarding the use of empirical potentials is their limited transferability: it is difficult to construct accurate potentials for alloy systems containing non-metallic elements, such as the Ni–C system mentioned above. Issues related to magnetism are also not commonly accessible via these methods. To address more complicated materials, theoretical insight has therefore increasingly relied upon first-principles simulations based on density functional theory (DFT) [15,16]. For the most part, previous DFT calculations have focused on the energetics of boundaries [17–20] and the impact of solute segregation upon intergranular cohesion [21–23]. For example, a series of studies by Freeman and co-workers (see [22] and references therein) have investigated the embrittling effects of various alloying agents upon Ni and Fe GBs. First-principles investigations of GB diffusion [24,25] are less common, due in part to the high computational cost of evaluating migration energy barriers. A recent study by Stumpf et al. [24] considered oxygen migration along a Pt Σ5 GB, and found no indication of anisotropic diffusion. However, EAM simulations [13] of interstitialcy (self)- migration in the same Σ5 GB in Cu have found that diffusion should be significantly faster in directions parallel to the [0 0 1] tilt axis.

Here, we present an ab initio study of C interstitial segregation to, and diffusion within, a Ni Σ3 symmetric tilt GB. From an applications perspective, the Ni–C system serves as a prototype for the class of interstitial alloys comprising austenitic steels. Other uses include electrodeposits and micro electro-mechanical systems (MEMS), where C is incorporated via organic precursors such as saccharin ($C_7H_4NO_3S$) [26]. The specific {1 1 2} boundary we consider here is a commonly occurring element in the microstructure of highly twinned, nanocrystalline Ni-based electrodeposits [27–29].

From a more fundamental perspective, many basic properties of grain boundaries remain incompletely understood. For example, while experiments [4,3] on symmetric tilt boundaries have shown that self-diffusion is generally faster parallel to the tilt axis, recent simulations [14] have found no such trend. Although an earlier study [30] has established the connection between bulk magnetism and the *surface* segregation of impurities, first-principles simulations of impurity segregation and diffusion at GBs in magnetic materials have yet to be reported.

The primary goals of this study are: (1) to determine if C segregation to the Ni Σ3 {1 1 2} GB is favorable; (2) to investigate the anisotropy of C GB diffusion, and (3) to identify whether Ni magnetism alters GB segregation and diffusion, indicating different behavior above and below the Curie point. To identify the equilibrium segregation geometry, we consider several ordered structures of GB-segregated C with "coverages" of 0.25, 0.5, 0.75 and 1 monolayers (ML). (The coverage is defined in terms of the fractional occupancy of GB trigonal prism sites.) Based on the calculated heats of segregation, the most favorable structure for segregated C has a "checkerboard" geometry with a (local) coverage of 0.5 ML. Nickel ferromagnetism acts as an additional driving force for GB segregation, in a similar fashion to what was observed for surface segregation [30]. Next, using transition-state-finding techniques based on the nudged elastic band method [31], we carefully map out the energy landscape for C GB diffusion between segregation sites along three pathways, drawing comparisons between results obtained for Ni in the non-magnetic and ferromagnetic states. Based on the relative sizes of the energy barriers for atom migration (E_a), we conclude that diffusion within this GB should be highly anisotropic, with very fast diffusion (relative to lattice diffusion) occurring along the $[1\ \bar{1}\ 0]$ tilt axis. For the most part, Ni magnetism was found to have only a small impact upon the size of the calculated barriers. Finally, we briefly investigate the influence of GB coverage upon E_as, and show that – at least for the specific mechanism considered here – a higher coverage impedes diffusion only slightly.

2. Computational details

Our density functional [15,16] calculations were performed with the VASP code [32], which uses a planewave basis for expansion of the electronic wavefunctions, and ultrasoft pseudopotentials [33,34] to replace the computationally expensive, yet chemically inert, core electrons. Brillouin zone sampling was performed using eight irreducible k-points generated from a $4 \times 1 \times 4$ Monkhorst–Pack grid [35], which produced heat of segregation values converged to within 0.02 eV. Electronic occupan-

cies were determined according to a Methfessel–Paxton scheme [36] with an energy smearing of 0.1 eV. The generalized gradient approximation (GGA) of Perdew and co-workers [37] (PW91) was used for the exchange-correlation energy, and planewave convergence testing revealed that a 290-eV cutoff was sufficient to converge total energies to within 1 meV/atom. In an earlier study [38], we calculated the heat of solution, activation energy for C lattice diffusion, and C–C binding energy for the bulk Ni–C system, and found very good agreement with experimental data, validating our theoretical technique. In this study we explore the influence of the magnetic state of Ni upon C GB segregation and diffusion by comparing results obtained with spin-polarized (ferromagnetic) and spin-averaged (non-magnetic) calculations. The ferromagnetic calculations are representative of the room- and low-temperature ($T < T_{\text{Curie}} \approx 627$ K) properties of Ni, while the high-temperature regime is approximated by the non-magnetic configuration.

3. Model geometry

The $\Sigma 3$ $(1\,1\,\bar{2})$ $[1\,\bar{1}\,0]$ symmetric tilt GB was constructed by first cleaving an FCC Ni lattice along a $\{1\,1\,2\}$ plane. One half of the separated crystal was then rotated 180° about an axis normal to this plane. Re-joining the two grains after the removal of overlapping boundary atoms produced the desired $\Sigma 3$ structure. The resulting GB supercell has orthorhombic symmetry (Fig. 1), with lattice vectors aligned with the $\langle 1\,1\,0\rangle$, $\langle 1\,1\,2\rangle$, and $\langle 1\,1\,1\rangle$ crystallographic directions, with respective lengths of $2\frac{a}{\sqrt{2}}$, $20\frac{a}{\sqrt{6}}$, and $3\frac{a}{\sqrt{3}}$, where $a = 3.525$ Å is the bulk lattice constant obtained from a separate primitive cell calculation. This geometry amounts to a 2×1 in-plane replication of the minimum GB structural unit, and consists of 48 Ni atoms, four $\{2\,2\,0\}$ planes, and three $\{1\,1\,1\}$ planes, respectively (see Figs. 1 and 2(a)). Normal to the boundary each grain consists of six $\{2\,2\,4\}$ planes which are terminated with free $\{1\,1\,2\}$ surfaces and a ~10 Å vacuum region. The dimensions of the supercell were fixed during the course of the simulations, however, all atomic coordinates were relaxed to a force tolerance of 0.05 eV/Å. (For the diffusion calculations the free surface atoms were constrained to the positions obtained during the previous segregation relaxations.)

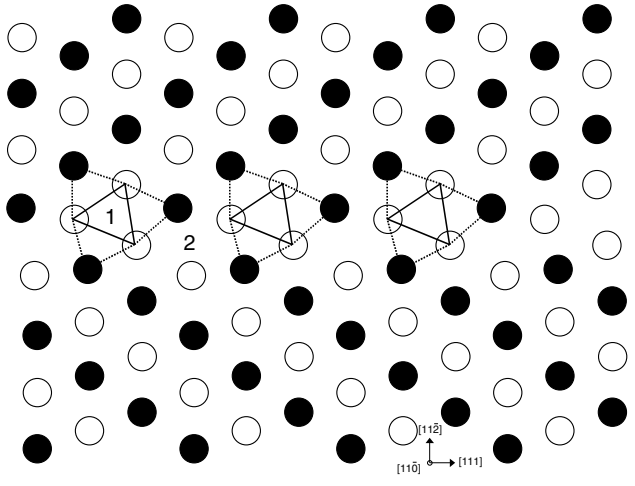

Fig. 1. Ni $\Sigma 3$ $(1\,1\bar{2})$ $[1\bar{1}0]$ tilt grain boundary. In this projection, the $[1\,\bar{1}\,0]$ tilt axis is normal to the plane of the page, and the supercell has been replicated four times along $[1\,1\,1]$. Black and white circles represent Ni atoms in alternate $\{2\,2\,0\}$ planes, and the capped trigonal prisms which constitute the GB structural units are outlined with solid (prisms) and dotted (caps) lines. The two most favorable sites for C occupation are identified as "1" and "2". See also Fig. 2

The relaxed GB structure in the absence of C is shown in Fig. 1, where filled/empty circles represent alternate $\{2\,2\,0\}$ planes, and the GB plane runs horizontally through the center of the figure. There is a slight displacement of the grains across the boundary of about $\frac{a}{3\sqrt{3}}$ along $[1\,1\,1]$, which is in reasonable agreement with previous computational [20,39,40] and experimental [40–43] structural determinations. [1] The zero Kelvin boundary energy was calculated [2] to be 837 and 866 mJ/m^2 for the NM and FM states, respectively, in good agreement with earlier EAM calculations [39]. The atomic structure at the boundary differs from the bulk FCC ordering, and can be described in terms of repeating capped trigonal prisms, as illustrated in Fig. 1. The two favorable sites for C occupation (see below) are located within the trigonal prisms, and are indicated with the numbers "1" and "2." (For clarity, only the capped trigonal prism surrounding site 1 is shown in Fig. 1.) Since our GB supercell is replicated along $[1\,\bar{1}\,0]$, there are two additional equivalent sites per cell displaced along $[1\,\bar{1}\,0]$ by a distance of $\frac{a}{\sqrt{2}}$. We distinguish these equivalent sites as $1a$ and $1b$, or $2a$ and $2b$; see Fig. 2(a) for an illustration of these sites.

4. Grain boundary segregation

Our segregation calculations employ 1–4 C atoms per supercell, resulting in a C concentration of 2–7.7 at.% for the entire cell. Based on the fractional occupancy

[1] The relaxed GB structure was determined by a partial gamma surface calculation, in which the grains were incrementally offset along $\langle 1\,1\,1\rangle$, followed by relaxation of all atomic coordinates along directions normal to $\langle 1\,1\,1\rangle$. High resolution transmission electron microscopy has found similar atomic structures for this boundary in Al [40,41], Au [42], and Pt [43]. In Ni the structure is believed to be the same, but to our knowledge has not yet been imaged.

[2] The boundary energy was estimated using a supercell containing 2 GBs and no vacuum region. The cell dimension normal to the boundary plane was optimized: the separation between GBs was ≈16.7 Å.

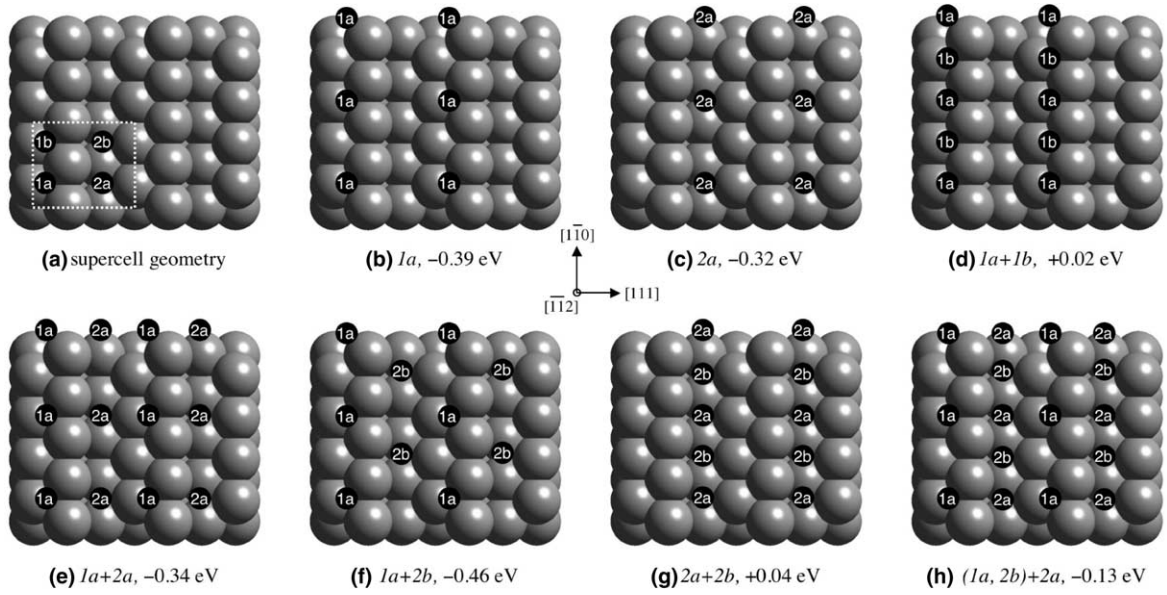

Fig. 2. Expanded view of the GB along a direction perpendicular to the (1 1 $\bar{2}$) boundary plane; atoms above the plane have been removed for clarity. The area of the supercell is indicated with a dotted rectangle in panel (a), along with the four favorable C segregation sites: 1*a*, 1*b*, 2*a*, and 2*b*. Panels (b) through (h) illustrate some of the (unrelaxed) configurations of GB-segregated C, and the corresponding (relaxed) average FM heats of segregation, $\Delta H_{\text{seg}}^{\text{avg}}$ (see Table 1 and Eq. (2)). The most favorable of these structures is the "checkerboard" configuration, panel (f).

of trigonal prism GB sites (see below), this concentration range is equivalent to a GB coverage (θ) of either 0.25, 0.5, 0.75, or 1 ML of C, respectively. The likelihood for GB segregation was assessed by calculating the incremental heat of segregation ($\Delta H_{\text{seg}}^{\text{inc}}$), defined as:

$$\Delta H_{\text{seg}}^{\text{inc}} = E_{\text{tot}}(C_{\text{GB}}^{N}) - E_{\text{tot}}(C_{\text{GB}}^{N-1} + C_{\text{bulk}}), \tag{1}$$

where $E_{\text{tot}}(C_{\text{GB}}^{N})$ is the total energy of a relaxed-ion supercell with N C interstitials at the GB, and $E_{\text{tot}}(C_{\text{GB}}^{N-1} + C_{\text{bulk}})$ is the equivalent energy for a supercell containing $N-1$ C atoms at the GB and one C atom at a bulk-like octahedral [38] interstitial site. To facilitate comparisons with other segregation studies we also tabulate the average heat of segregation ($\Delta H_{\text{seg}}^{\text{avg}}$) per C atom, defined as the difference in energy between N C atoms in the GB vs. in bulk solid solution: $\Delta H_{\text{seg}}^{\text{avg}} = \frac{1}{N}[E_{\text{tot}}(C_{\text{GB}}^{N}) - E_{\text{tot}}(C_{\text{bulk}}^{N})]$. Note that $\Delta H_{\text{seg}}^{\text{avg}}$ can be obtained from $\Delta H_{\text{seg}}^{\text{inc}}$ according to

$$\Delta H_{\text{seg}}^{\text{avg}} = \frac{1}{N}\sum_{i=1}^{N} \Delta H_{\text{seg}}^{\text{inc}}(N,i), \tag{2}$$

where $\Delta H_{\text{seg}}^{\text{inc}}(N,i)$ is the incremental heat of segregation for the ith C atom, leading up to a specific N-atom GB coverage. For example, $H_{\text{seg}}^{\text{avg}} \times N$ for the configuration in which C atoms occupy the 1*a* and 2*b* GB sites (Fig. 2(f), −0.92 eV FM) is given by $\Delta H_{\text{seg}}^{\text{inc}}$ to the 1*a* site (Fig. 2(b), −0.39 eV), plus $\Delta H_{\text{seg}}^{\text{inc}}$ to the 2*b* site taking the 1*a* site as occupied (−0.53 eV).

For this study, we assume that C occupies interstitial sites (C_{int}) both in the lattice and at the GB. This is a reasonable approximation considering the small atomic size of C relative to Ni (atomic radius of C, $R_{\text{C}} = 0.61 R_{\text{Ni}}$), and experimental evidence suggesting C is an interstitial in the lattice [44]. Furthermore, calculated (NM) formation energies for substitutional C (C_{sub}) in the lattice and GB are, respectively, 1.4 and 0.99 eV greater than for C_{int} in similar environments. [3] Optimization of the C_{sub} geometry (in both GB and lattice configurations) resulted in a large relaxation of the C away from the center of the substitutional site, where it adopted an "interstitial-like" coordination, indicating its relatively small size.

To identify possible segregation sites, we performed a preliminary search over 13 different GB positions using the primitive (1 × 1) cell geometry (24 Ni atoms), consisting of two {2 $\bar{2}$ 0} planes and taking Ni to be in the non-magnetic (NM) spin state. (This cell is half the size along [1 $\bar{1}$ 0] of the supercell depicted in Fig. 2(a).) Two favorable sites were identified, corresponding to positions 1 and 2 in Fig. 1 (i.e., sites 1*a* and 2*a* in Fig. 2(a)), both of which exhibit octahedral coordination upon relaxation. Next, the supercell dimension was doubled along [1 $\bar{1}$ 0], and $\Delta H_{\text{seg}}^{\text{inc}}$ was reevaluated for these two positions, assuming both NM and ferromagnetic (FM) states. Except where explicitly noted, our segregation and diffusion calculations used this 48 Ni atom 2 × 1 supercell, illustrated in Fig 2(a).

[3] The formation energy for C_{sub} at the GB was evaluated only for the most compressed GB site, which should be the most favorable site for substitution of the smaller C atom.

Table 1
Average (ΔH_{seg}^{avg}) and incremental (ΔH_{seg}^{inc}) heats of segregation (in eV) to specified GB sites as a function of magnetic state and C coverage

Site(s)	C Coverage, θ	ΔH_{seg}^{avg} NM	ΔH_{seg}^{avg} FM	ΔH_{seg}^{inc} NM	ΔH_{seg}^{inc} FM
1*a*	0.25	−0.26	−0.39	−0.26	−0.39
2*a*	0.25	−0.23	−0.32	−0.23	−0.32
1*a* + 1*b*	0.5	0.24	0.02	0.73	0.42
1*a* + 2*a*	0.5	−0.17	−0.34	−0.08	−0.28
1*a* + 2*b*	0.5	−0.28	−0.46	−0.29	−0.53
2*a* + 2*b*	0.5	0.20	0.04	0.63	0.40
(1*a*, 2*b*) + 2*a*	0.75	0.08	−0.13	0.79	0.52
(1*a*, 2*b*) + 1*b*	0.75	0.13	−0.14	0.95	0.49
(1*a*, 2*b*, 2*a*) + 1*b*	1	0.35	0.10	1.15	0.79

Segregation sites are described using the notation "occupied site(s) + target segregation site". For example, ΔH_{seg}^{inc} for the (1*a*, 2*b*) + 2*a* configuration (Fig. 2(h)) gives the heat of segregation to a 2*a* site, with sites 1*a* and 2*b* occupied as in Fig. 2(f). ΔH_{seg}^{avg} is defined in Eq. (2).

We focus first on the segregation of an isolated C atom, for which heat of segregation data are reported in the first two rows of Table 1. Note that ΔH_{seg}^{inc} values for the *xa* (Fig. 2(b)) and *xb* sites ($x = 1,2$) are equal by symmetry; for simplicity, we therefore report data for *a*-type sites only.

As shown in Table 1, ΔH_{seg}^{inc} for the 1*a* and 2*a* sites ($\theta = \frac{1}{4}$) are negative and roughly similar for a given magnetic state: about −0.25 eV in the NM state, and −0.35 eV in the FM state, with site 1 being slightly preferred over site 2 by approximately 30 and 70 meV, respectively. Neglecting entropic contributions, sites for which $\Delta H_{seg}^{inc} < 0$ would be candidates for GB segregation. Tests performed on a supercell with a doubled dimension along $[1\ \bar{1}\ 0]$ (96 Ni atoms, $\theta = \frac{1}{8}$) indicate that ΔH_{seg}^{inc} for the present case ($\theta = \frac{1}{4}$) capture segregation energies for the low-coverage limit rather well. For example, ΔH_{seg}^{inc} to the 1*a* site at $\frac{1}{8}$ ML (−0.23 eV NM, −0.41 eV FM) differs from the $\frac{1}{4}$ ML value by at most 0.03 eV. The magnitude of ΔH_{seg}^{inc}, falling in the range of −0.25 to −0.35 eV, would place this system in the moderate- to strongly segregating regime. [4]

The heat of segregation is generally more negative in the FM state, suggesting that Ni ferromagnetism provides an additional driving force for GB segregation. This *magnetically enhanced* segregation can be understood by examining the impact of the C interstitial upon the Ni magnetization. In two earlier studies [30,38], we demonstrated that C interstitials disrupt Ni ferromagnetism, partially suppressing the magnetic moments of adjacent Ni atoms and reducing the total moment of the supercell. This disruption is energetically unfavorable. In Table 2, we report the total supercell magnetic moment and the average moments on Ni atoms nearest-neighbor (NN) to the C interstitial, for C at various positions in the GB supercell. The addition of a C interstitial reduces the total magnetic moment of the clean

[4] Conventionally, $\Delta H_{seg} \gtrsim -0.1$ eV corresponds to weak segregation, while strong segregation is characterized by $\Delta H_{seg} \lesssim -0.4$ eV.

Table 2
Total supercell magnetic moment, average moment for Ni atoms nearest-neighbor (NN) to C, and average Ni–C bond length for the clean (C-free) GB, and for three GB supercells with an interstitial C in various positions

GB	Supercell	Average NN	Average Ni–C
Configuration	Mag. (μ_B)	Ni Mag. (μ_B)	Bond length (Å)
Clean GB	30.79		
C in bulk	27.45	0.21	1.85
C at 1*a*	28.35	0.35	1.95
C at 2*a*	28.00	0.27	1.90

The magnetic moment of a bulk-like Ni atom was calculated to be $0.65\mu_B$.

(C-free) supercell of $30.8\mu_B$ by 2.4–$3.3\mu_B$, depending on C position. This fact is reflected by the atomic moments of the Ni atoms NN to the C, which are suppressed to 0.21–$0.35\mu_B$ from the C-free value of about $0.65\mu_B$.

Table 2 also illustrates that the C's disruption of magnetism is largest when at a bulk site, where the total moment is reduced by $3.3\mu_B$ relative to the C-free case. The disruption is reduced when C segregates to either of the favorable GB sites, resulting in smaller magnetization reductions of 2.4 and $2.8\mu_B$ for sites 1*a* and 2*a*, respectively. The magnetic enhancement of the heat of segregation is most pronounced for the 1*a* site, which is consistent with this site having the smallest reduction in total magnetization. The size of the FM enhancement to ΔH_{seg}^{inc}, −130 meV for site 1*a* and −90 meV for site 2*a*, is of the correct order of magnitude given each site's change in supercell magnetization (relative to the bulk site), and the calculated magnetization energy of bulk Ni, $E_{mag} \approx 55$ meV/atom [38].

It is likely that the C's impact upon magnetism is reduced when at the GB because the boundary is a region of excess free volume, allowing for a more natural adoption of Ni–C bonding without the compressive stresses characterizing the smaller sites within the lattice. As can be seen in Table 2 the average Ni–C bond length at the GB is larger than in the bulk. Bond lengths are

also largest for the 1*a* site, which has the greatest total moment of any of the C-containing supercells.

Carbon segregation in FM Ni could also be enhanced if the boundary plane was inherently non-magnetic or only weakly ferromagnetic.

To examine this possibility we evaluated the site-projected moments within the C-free supercell. No difference in magnetization at the GB was observed relative to that for bulk-like atoms, suggesting that this effect is not relevant here. [However, we did find enhanced moments of $\sim 0.71\mu_B$ at the {1 1 2} free surfaces (relative to a $0.65\mu_B$ moment in bulk), consistent with previous studies of surface magnetism [45].]

An additional topic of interest concerns the equilibrium atomic structure and coverage of GB-segregated C. To explore this issue we have calculated the heats of segregation of several ordered GB structures with C coverages of 0.25, 0.5, 0.75, and 1 ML. (Disordered structures are not considered here due to computational limits on the size of our supercell.) Rows 3–9 of Table 1 list heats of segregation for coverages in the range $0.5 \leqslant \theta \leqslant 1$. The unrelaxed structures corresponding to most of these configurations are illustrated in Fig. 2. To estimate the equilibrium coverage we focus on ΔH_{seg}^{inc}; in principle, segregation will stop when the addition of C to the GB becomes energetically unfavorable, i.e., when $\Delta H_{seg}^{inc} > 0$. [5] For $\theta > 0.25$ ML, ΔH_{seg}^{inc} is negative only for the $1a + 2a$ and $1a + 2b$ geometries at $\theta = 0.5$, suggesting that segregation is unlikely for $\theta > 0.5$ ML. Although there appear to be no experimental measurements of C segregation to the present {1 1 2} boundary, atom probe field-ion microscopy has reported high C concentrations of 25–35 at.% at two Ni GBs of unknown orientation [6]. This observation is in good agreement with our predicted level of segregation (0.5 ML), which, when expressed in terms of the atomic density of the {1 1 2} boundary plane, is equivalent to 25 at.% C.

Of the ordered structures considered here, the most favorable configuration for GB-segregated C is the $1a + 2b$ "checkerboard" geometry of Fig. 2(f), which has the most negative ΔH_{seg}^{avg} (Eq. (2) of all candidate structures: $\Delta H_{seg}^{avg} = -0.28$ eV (NM), -0.46 eV (FM). Segregation to $2b$ sites is stronger in the presence of occupied $1a$ sites [$\Delta H_{seg}^{inc} = -0.53$ eV (FM)], relative to isolated type-2 sites [$\Delta H_{seg}^{inc} = -0.32$ eV (FM)]. Based on these energetics, the behavior of C at this GB is expected to be similar to that of an ordered adsorbate layer on a surface. For $\theta < 0.5$, GB C will preferentially exist as checkerboard "islands" whose coverage of the boundary plane will grow in proportion to the amount of segregated C. Although this checkerboard structure may contain a significant number of random vacancies, an investigation of vacancy effects would require calculations on large supercells, which has not been done here.

5. Grain boundary diffusion

As with lattice diffusion, GB diffusion is commonly described in terms of an Arrhenius expression,

$$D = D_0 \exp\left(\frac{-E_a}{k_B T}\right). \tag{3}$$

Here D is the diffusivity, D_0 is the exponential prefactor, E_a is the activation energy for atom migration, k_B the Boltzmann factor, and T is the absolute temperature. Our focus here is on calculating E_a for the diffusion of C interstitials between favorable segregation sites at the GB. Since the magnitude of the diffusivity is largely determined by E_a, knowledge of these barriers would allow an assessment of whether GB diffusion is faster than in the bulk lattice. Furthermore, the possibility of anisotropic GB diffusion can be explored by mapping out the activation energy profiles for migration along orthogonal directions in the boundary plane.

The instantaneous energies and atomic geometries as a function of C position along a given diffusion pathway were evaluated using large-scale nudged elastic band (NEB) calculations [31]. In this method, a series of system images trace the path between predefined local minima on the potential energy surface. In the present case, the local minima endpoints were taken to be favorable segregation sites, and the initial intermediate images were generated through linear interpolation. [6] The minimum energy path between endpoints was then determined by minimizing the atomic forces on each image (to a tolerance of 0.05 eV/Å via the quick-min algorithm,) normal to the local hypertangent. The images are coupled via a fictitious spring force having a non-zero component parallel to the hypertangent. In combination, this relaxation scheme prevents so-called corner-cutting and image agglomeration [31]. Moreover, the forces projected along the hypertangent at each image can be used to refine the estimate of E_a through spline interpolation. Although our supercell contains only a moderate number of atoms (49), the NEB calculations performed here required a large number of images to accurately resolve the multiple maxima encountered along some of the

[5] An alternative measure of C concentration at the GB could be achieved with a properly parameterized empirical potential and Monte-Carlo simulations, as done for Ni–Cu in [11], however this has not been done here.

[6] It was necessary to manually adjust the initial NEB geometries in cases where linear interpolation generated images with small distances between adjacent atoms.

Table 3
Activation energies (E_a) for C interstitial diffusion between specified sites in the GB and between adjacent octahedral sites in the bulk lattice, assuming a C GB coverage of $\frac{1}{4}$ ML

Endpoints	Direction relative to tilt axis	E_a NM (eV)	E_a FM (eV)
$1a \rightarrow 1b$	$\parallel$	0.77	0.73
$2a \rightarrow 2b$	$\parallel$	0.44	0.44
$1a \rightarrow 1a$	$\perp$	1.72	1.92
Bulk [38]		1.62	1.60

For the $1a \rightarrow 1a$ pathway only the largest E_a is listed.

pathways; using 16 simultaneous images resulted in a large calculation containing 784 atoms.

We examined three pathways for C interstitial migration within the GB plane, as summarized in Table 3. Two pathways were taken as parallel to the $[1\ \bar{1}\ 0]$ tilt axis, $1a \rightarrow 1b$ and $2a \rightarrow 2b$, while the other pathway was normal to the tilt axis (along [1 1 1]), and used equivalent $1a$ sites as endpoints ($1a \rightarrow 1a$). [7] The C GB concentration was initially set at $\frac{1}{4}$ ML. Due to the modest size of our supercell along $[1\ \bar{1}\ 0]$ we expect C–C image interactions to have an effect on calculated E_as comparable in size to the difference in ΔH^{inc}_{seg} between $\theta = 0.25$ and $\theta = 0.5$ (i.e., a few tens of meV). For each pathway we determined the impact of Ni magnetism upon the E_as by first performing a NM NEB calculation, followed by an equivalent FM calculation.

The results of our GB NEB calculations are illustrated in Fig. 3, where we simultaneously plot the total energy (left ordinate, for both NM and FM calculations) and total magnetization (right ordinate) as a function of hyperdistance along each diffusion pathway. For comparison, we also include data from our earlier study of C diffusion between bulk octahedral sites; [38] see also Table 3. Considering first the NM pathways along the tilt axis (depicted by solid lines and filled circles in the top panel of Fig. 3), we find relatively small E_as: 0.77 eV for $1a \rightarrow 1b$, and 0.44 eV for $2a \rightarrow 2b$. As expected, the energy profiles are symmetric about their midpoints since a mirror plane bisects the $[1\ \bar{1}\ 0]$ path. In comparison to lattice diffusion, for which our calculations predict $E_a = 1.62$ eV, the rate of GB diffusion along the tilt axis should be significantly faster. This is in reasonable agreement with the experimental trends observed by Parthasarathy and Shewmon [5], who found that at 600 °C carbon diffuses along Ni GBs four orders of magnitude faster than in the lattice.

That the $2a \rightarrow 2b$ pathway has a relatively lower E_a can be understood in terms of the coordination of the C atom at the transition state and strain on the Ni lattice. First, we have already established [38] that the preferred C sites, both in the lattice and at this GB, are highly coordinated (octahedral) sites. The atomic geometry of the $2a \rightarrow 2b$ path most faithfully maintains this high-coordination preference: at the transition state this path is 5-fold coordinated, while the $1a \rightarrow 1b$ path is tetrahedrally coordinated. In addition, the atomic relaxation energy expended in straining the Ni lattice at the $1a \rightarrow 1b$ transition state (relative to that of the initial segregation site) is 0.13 eV larger than for the $2a \rightarrow 2b$ pathway.

From a phenomenological standpoint, GB diffusion and segregation appear to be correlated phenomena, as strongly attractive segregation sites – deep minima on the potential energy surface – often exhibit slower rates of GB diffusion through the so-called "trapping" effect [2]. While our prediction of larger E_a for the more-strongly bound $1a$ site (relative to $2a$) is qualitatively consistent with this notion, the excess binding energy of this site (0.07 eV FM, 0.03 eV NM) is too small to account for the large ~0.3 eV difference in E_a for $[1\ \bar{1}\ 0]$-directed migration. An additional mechanism for trapping could arise from the condensation of segregated C into checkerboard islands, since detachment from an island is an endothermic process.

In contrast to the low-energy $[1\ \bar{1}\ 0]$ pathways, the (NM) pathway perpendicular to the tilt axis (Fig 3, bottom panel) is characterized by larger activation energies, and is significantly more complicated, exhibiting four energy barriers along the reaction coordinate. This path is also nearly three times longer, reflecting both the greater distance between the NEB endpoints, and the substantial degree of atomic relaxation accompanying the migration. Fig. 4 depicts the atomic configuration at various points along this pathway. As expected, there is a low-energy channel about half-way through (7–9 Å) the migration, where the C passes through site 2 (see Fig. 4(e) and (f)). The largest energy barriers occur near the beginning and end of the path, corresponding to configurations where C traverses the energetically unfavorable (low free-volume) cap sites (see Fig. 4(b) and (g)). The largest barrier of $E_a = 1.72$ eV occurs at the end of the migration, and is comparable in size to that of lattice diffusion. The atomic configurations corresponding to this barrier are shown in Fig. 4(g) and (h), and are characterized by a slight canting of the grains, despite the fact that the atoms far from the boundary were held fixed. [8] This effect is most likely an artifact of our relatively small supercell. In the limit of an infinitely large supercell, we would not expect to see such collective behavior, since the interior portions of the grains would be relatively immobile. We therefore expect that the

[7] For this path a C interstitial at site $1a$ traverses the full length of the supercell along [1 1 1], passing by the $2a$ site, until finally reaching its image site in the adjacent supercell.

[8] Releasing the fixed atoms results in an even larger canting – which we believe is unphysical – and a substantial decrease in E_a to about 1 eV.

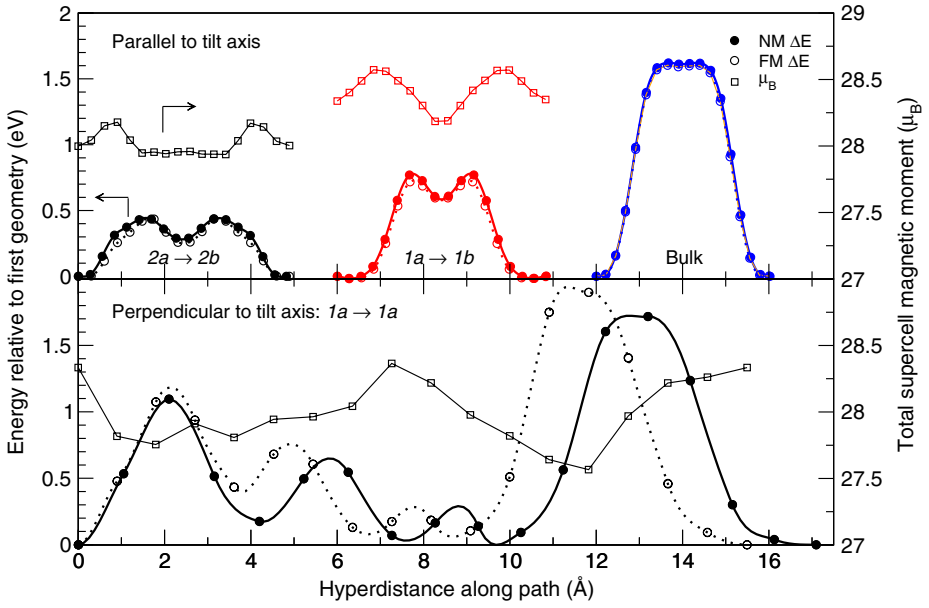

Fig. 3. Activation energies (circles, left ordinate) and total supercell magnetic moments (squares, right ordinate) for interstitial C diffusion along three pathways within the Ni Σ3 GB and in bulk Ni, as calculated with the nudged elastic band method. The energy zero for each pathway is set to the formation energy of its initial geometry. Data for bulk diffusion is taken from [38].

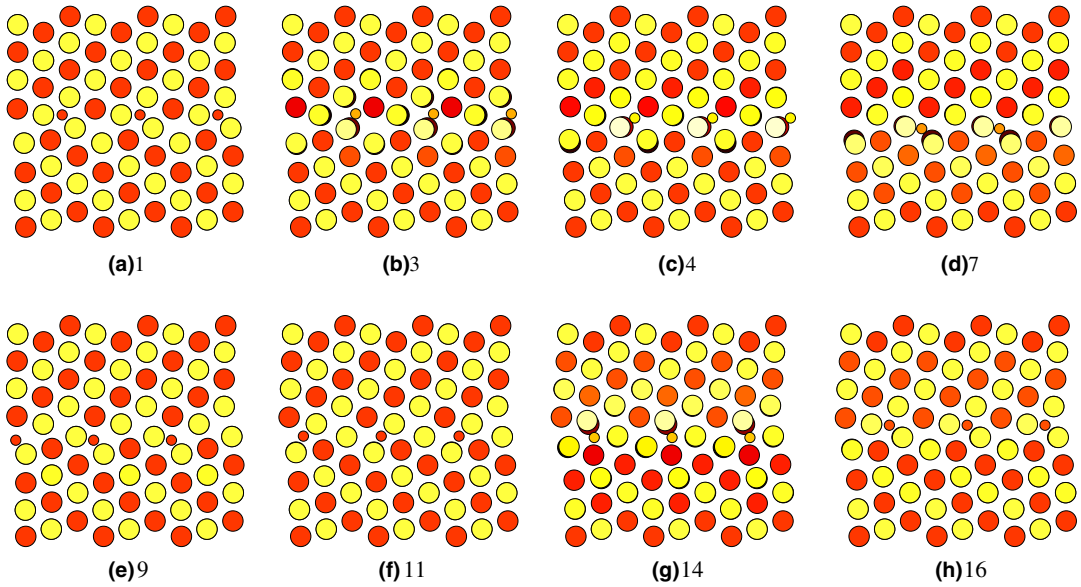

Fig. 4. Atomic structure of the Ni Σ3 GB at various stages along the $1a \rightarrow 1a$ C diffusion pathway, perpendicular to the tilt axis. The position of the C atom is given by the small circle, and the atoms are color-coded to reflect their displacement along [1 $\bar{1}$ 0], which is normal to the page. In this projection, the C migrates from left to right along [1 1 1]. The caption gives the corresponding image number from the energy profile in Fig. 3, lower panel.

calculated E_a for this barrier is a lower bound to the true E_a.

Based on the substantial difference in E_as for GB diffusion along these perpendicular paths – at least 1 eV in the NM state – our calculations predict a large anisotropy in diffusivity for this model GB. Diffusion along ⟨1 1 0⟩ "channels" should be much faster than lattice diffusion, while diffusion along [1 1 1] should be slower. Of course the diffusivity in a real GB depends upon the local defect concentration, which would likely moderate this effect somewhat. Nevertheless, it is instructive to see how large the anisotropy could be in an ideal case.

From a practical standpoint, the possibility of fast diffusion along the tilt axis could impact the surface composition of highly ⟨1 1 0⟩-textured films, such as those being investigated for use in MEMS. In particular,

electrodeposited Ni–Mn alloys (with greater than 0.2 wt% Mn) exhibit a ⟨1 1 0⟩ texture parallel to the growth direction [46], and are also known to have a microstructure containing the Σ3 boundary discussed herein [27]. The small E_as found here for GB diffusion along ⟨1 1 0⟩ could lead to enhanced mass transport along the columnar grains, facilitating surface segregation.

Shifting focus now to the ferromagnetic NEB calculations, Fig. 3 plots both the FM energy profiles (open circles) and total supercell magnetic moments (squares) as a function of hyperdistance for each of the GB diffusion pathways. For the most part, the addition of Ni ferromagnetism results in only a small change to the NM E_as, consistent with earlier theoretical [38] and experimental [47] studies of lattice diffusion. For diffusion parallel to the tilt axis, the FM change to the $1a \rightarrow 1b$ E_a is about 40 meV, while for the $2a \rightarrow 2b$ path the change is negligible (see Table 3). In both cases, the shape of the energy profile is virtually unchanged. This insensitivity to magnetism is to a large extent duplicated for the [1 1 1] path, where the heights of the first three barriers are similar to those found in the NM calculation. However, there is an increase of 0.2 eV for the fourth (and largest) E_a which coincides with the C passing between the most compressed GB sites. The general shape of this pathway is also similar to that found for the NM state. Overall, the appearance of large energy barriers coincides with minima in the total magnetization.

Because C disrupts Ni ferromagnetism [30], and changes in C coordination in the course of diffusion could in principle alter this disruption, one might expect a substantial change in E_a profiles upon inclusion of spin polarization effects. That this is not the case can be understood by recalling that Ni has a relatively small magnetization energy, $E_{mag} \approx 55$ meV. (The calculated GGA magnetic moment in fcc Ni is $0.62\mu_B$ [38]). Therefore, a large change in magnetization, similar to completely extinguishing the moments on two atoms, would be needed to alter energetics by about 0.1 eV. As illustrated in Fig. 3, the supercell magnetic moment (M_{tot}) varies by less than 3% ($<1\mu_B$) as a function of hyperdistance across all pathways. The combination of these two effects – Ni's small E_{mag} and small variations in M_{tot} – results in E_as which are largely unchanged by Ni magnetism.

Finally, we have briefly considered the effect of segregant concentration upon E_a: that is, do higher coverages of segregated C retard GB diffusion? Earlier we referred to the notion that strongly attractive GB sites generally exhibit slower rates of GB diffusion, which is in qualitative agreement with our calculated E_as for diffusion along the tilt axis at $\theta = \frac{1}{4}$. On the other hand, large (negative) heats of segregation could result in a high solute enrichment in the boundary region, which would slow diffusion through "stuffing" of the GB [2].

To explore the coverage dependence of GB diffusion we have re-evaluated the ⟨1 1 0⟩-directed $2a \rightarrow 2b$ diffusion pathway with the $1b$ site occupied ($\theta = 0.5$). For both magnetic states, we find that the shapes of the energy profiles are similar to that of Fig. 3 (top left), however, there is a small increase in the second E_a peak of about 0.1 eV which appears as the diffusing C approaches the occupied $1b$ site. This suggests that while higher concentrations of segregated C may impede GB diffusion, the coverage effect is weak for this diffusion mechanism.

6. Conclusion

We have used density functional theory to study the segregation and diffusion of C interstitials at a Ni Σ3 GB. The impact of Ni magnetism was assessed by comparing results for the heat of segregation and diffusion energy barriers (E_a) with, and without, spin polarization. For segregation to a C-free boundary, we identified two unique GB sites with favorable segregation energies of about −0.25 eV in the NM Ni state, and −0.35 eV in the FM state. Segregation is generally enhanced by 0.1–0.2 eV in the FM state because C interstitials suppress Ni ferromagnetism – an energetically unfavorable process – and this effect is minimized for sites at the GB relative to sites in the lattice. By examining several ordered structures, we identified a "checkerboard" geometry as the most favorable configuration for GB-segregated C, with a heat of segregation approaching −0.5 eV/C atom (FM).

Large-scale nudged elastic band calculations were used to evaluate E_as for C GB diffusion along three pathways between favorable segregation sites, at a coverage approximating isolated C atoms. Based on the relative sizes of E_a, GB diffusion is predicted to be highly anisotropic. Migration parallel to the tilt axis exhibited E_as less than half the size (0.44 and 0.77 eV) found for lattice diffusion (1.62 eV), consistent with experimental reports of fast GB diffusion in Ni–C alloys [5]. In contrast, E_as perpendicular to the tilt axis were comparable to the lattice E_a. Diffusion in the presence of higher levels of segregated C ($\frac{1}{2}$ ML) was characterized by a small (≈0.1 eV) increase in activation energy, and should therefore be slightly slower. Unlike segregation, which is sensitive to magnetic effects, diffusion energy barriers were found to be (with one exception) largely independent of the Ni magnetic state.

Acknowledgements

This work was supported by the US Department of Energy, in part by the Office of Basic Energy Sciences, Division of Materials Sciences, under contract number

DE-AC04-94AL85000. We thank G. Lucadamo and R. Stumpf for reviewing a preliminary version of this report.

References

[1] Sutton AP, Balluffi RW. Interfaces in crystalline materials. Oxford: Oxford University Press; 1995.
[2] Mishin Y, Herzig C. Mater Sci Eng A 1999;260:55.
[3] Hoffman RE. Acta Metall 1956;4:97.
[4] Sommer J, Herzig C, Mayer S, Gust W. Defect Diff Forum 1989;66–69:843.
[5] Parthasarathy TA, Shewmon PG. Scripta Metall 1983;17:943.
[6] Alvensleben Lvon. J Phys Colloque C 1988;6:335.
[7] Ma Q, Liu CL, Adams JB, Balluffi RW. Acta Metall Mater 1993;41:143.
[8] Nomura M, Adams JB. J Mater Res 1995;10:2916.
[9] Liu X-Y, Xu W, Foiles SM, Adams JB. Appl Phys Lett 1998;72:1578.
[10] Farkas D. J Phys Condens Matter 2000;12:R497.
[11] Foiles SM. Phys Rev B 1989;40:11502.
[12] Rittner JD, Seidman DN. Acta Mater 1997;45:3191.
[13] Sørensen MR, Mishin Y, Voter AF. Phys Rev B 2000;62.
[14] Suzuki A, Mishin Y. Interf Sci 2003;11:131.
[15] Hohenberg P, Kohn W. Phys Rev 1964;136:B864.
[16] Kohn W, Sham LJ. Phys Rev 1965;140:A1133.
[17] Needles M, Rappe AM, Bristowe PD, Joannopoulos JD. Phys Rev B 1992;46:9768.
[18] Wright AF, Atlas SR. Phys Rev B 1994;50:15248.
[19] Lu G, Kioussis N, Ciftan M. Phys Rev B 1999;59:891.
[20] Hamilton JC, Foiles SM. Phys Rev B 2002;65:064104.
[21] Thomson DI, Heine V, Finnis MW, Marzari N. Phil Mag Lett 1997;76:281.
[22] Geng WT, Freeman AJ, Olson GB. Phys Rev B 2001;63:165415.
[23] Lu GH, Suzuki A, Ito A, Kohyama M, Yamamoto R. Phil Mag Lett 2001;81:757.
[24] Stumpf R, Liu C-L, Tracy C. Phys Rev B 1999;59:16047.
[25] Liu CL. Appl Phys Lett 2002;80:763.
[26] Elsherik AM, Erb U. J Mater Sci 1995;30:5743.
[27] Lucadamo G, Medlin DL, Yang NYC, Kelly JJ, Talin AA. Unpublished.
[28] Hall CR, Fawzi SAH. Phil Mag A 1986;54:805.
[29] Lin CS, Hsu PC, Chen CH. J Appl Electrochem 2001;31:925.
[30] Siegel DJ, van Schilfgaarde M, Hamilton JC. Phys Rev Lett 2004;92:086101.
[31] Jónsson H, Mills G, Jacobsen KW. Classical and quantum dynamics in condensed phase simulations. Singapore: World Scientific; 1998. p. 385.
[32] Kresse G, Furthmüller J. Phys Rev B 1996;54:11169.
[33] Vanderbilt D. Phys Rev B 1990;41:7892.
[34] Kresse G, Hafner J. J Phys: Condens Mater 1994;6:8245.
[35] Monkhorst HJ, Pack JD. Phys Rev B 1976;13:5188.
[36] Methfessel M, Paxton AT. Phys Rev B 1989;40:3616.
[37] Perdew JP, Chevary JA, Vosko SH, et al. Phys Rev B 1992;46:6671.
[38] Siegel DJ, Hamilton JC. Phys Rev B 2003;68:094105.
[39] Rittner JD, Seidman DN. Phys Rev B 1996;54:6999.
[40] Medlin DL, Mills MJ, Stobbs WM, Daw MS, Cosandey F. Mat Res Soc Symp Proc 1993;295:91.
[41] Dehm G, Inkson BJ, Wagner T. Acta Mater 2002;50:5021.
[42] Hetherington CJD, Dahmen U, Pennisson J-M. Mat Res Soc Symp Proc 1997;466:215.
[43] Ramanathan S, Clemens BM, McIntyre PC. Phil Mag A 2001;81:2073.
[44] Numakura H, Kashiwazaki K, Yokoyama H, Koiwa M. J Alloys Comp 2000;310:344.
[45] Aldén M, Mirbt S, Skriver HL, Fosengaard NM, Johansson B. Phys Rev B 1992;46:6303.
[46] Yang NYC, Headley TJ, Kelly JJ, Hruby JM. Scripta Mater 2004;51:761.
[47] Diamond S, Wert C. Trans Met Soc AIME 1967;239:705.